

*Supporting Information for*

## **Guest-Dependent Bond Flexibility in**

### **UiO-66, a “Stable” MOF**

Kevin Fabrizio,<sup>a</sup> Anastasia B. Andreeva,<sup>a</sup>

Kentaro Kadota,<sup>a</sup> Amanda J. Morris,<sup>b</sup> and Carl K. Brozek<sup>\*a</sup>

*<sup>a</sup>Department of Chemistry and Biochemistry, Material Science Institute,*

*University of Oregon, Eugene, OR 97403, United States*

*<sup>b</sup>Department of Chemistry, Virginia Tech, Blacksburg, VA 24060, United States*

Email: cbrozek@uoregon.edu

### **Table of Contents**

<b>Experimental methods</b>	S2
<b>UiO-66 synthesis and PXRD characterization</b>	S2
<b>Global Fitting Procedure</b>	S3
<b>DRIFTS</b>	S4
<b>Global Fittings</b>	S5
<b>Stability of UiO-66 with Et<sub>3</sub>N</b>	S7
<b>FWHM of Asymmetric Stretches under Vacuum</b>	S8
<b>Data and Global Fitting Results under Nitrogen</b>	S9
<b>Solvent-dependent flexibility constants</b>	S9
<b>References</b>	S10

## Experimental methods

**Materials.** All commercial chemicals were used as received unless stated otherwise: terephthalic acid (98%, Sigma Aldrich), zirconium(IV) chloride (99.5% trace metals basis, Beantown Chemical), concentrated hydrochloric acid (37%, ACS grade, Sigma Aldrich). The solvents used in all manipulations were rigorously dried using Schlenk technique and stored over molecular sieves in a nitrogen glovebox. N,N-dimethylformamide (DMF, ACS grade, Fisher Scientific) was collected from an SP-1 solvent purification system purchased from LC Technology Solutions Inc., and stored under a nitrogen atmosphere. The solvothermal synthesis of UiO-66 was either conducted in a 100-mL Duran Schott bottle, or an autoclave Parr bomb in a Yamato Convection Oven.

**Characterization.** Sample purity was verified by powder X-Ray diffraction (PXRD) with a Bruker D2 Phaser benchtop diffractometer. Variable-temperature diffuse reflectance infrared Fourier transform spectroscopy (DRIFTS) was performed on a Nicolet 6700 FT-IR spectrometer using a Transmission E.S.P. attachment paired with Harrick Scientific Praying Mantis Diffuse Reflection (DRP) accessory and MCT detector. A Harrick Scientific Low Temperature Reaction Chamber (CHC) that enabled introducing vacuum to the sample was equipped with UV quartz and 2 Harrick 15 × 2 mm potassium bromide windows. To maximize intensity, all samples were diluted with ground KBr. Reflectance FTIR spectra were collected in the range of 4000 – 650  $\text{cm}^{-1}$  with 2  $\text{cm}^{-1}$  resolution and 32 scans unless stated otherwise.

## UiO-66 synthesis

Adapted from Katz et. al,<sup>1</sup> zirconium(IV) chloride (0.126 g, 0.54 mmol) was dissolved in DMF (5 mL) in a 20-mL scintillation vial under inert atmosphere. Upon exposing the vial to atmospheric conditions, concentrated hydrochloric acid (1 mL) was added, and the mixture was sonicated for 20 minutes and transferred to 100-mL Schott jar with a Teflon ring. Terephthalic acid (0.1232 g, 0.74 mmol) and DMF (10 mL) were added to the same jar and sonicated for additional 20 minutes. After contents were fully dissolved, the jar was placed in a convection oven at 80 °C overnight (12 hours). The resulting white powder was washed with DMF (2 × 30 mL) and ethanol (2 × 30 mL) over the course of 2 days and dried at room temperature.

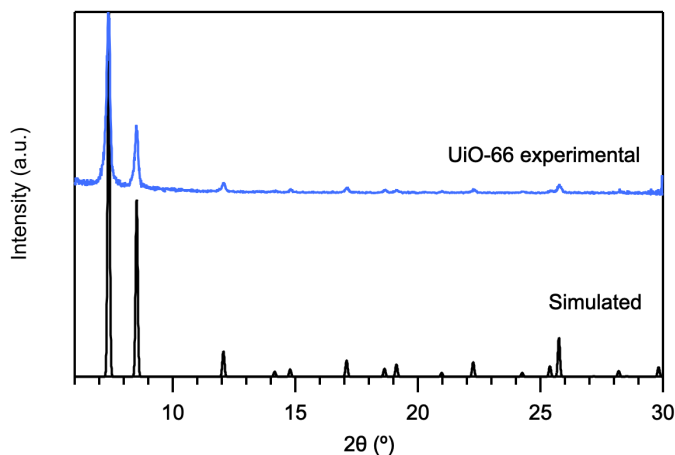


**Figure S1.** Experimental and simulated X-ray diffraction patterns of UiO-66.

### Global Fitting Procedure

As described in Ref. 3 and Ref. 4, the equilibrium model relies on a two Gaussian fitting in which peak position is held constant across a range of environmental conditions, and the peak width and area are allowed to shift.<sup>2,3</sup> All global fittings were performed in Origin Pro 2023 (10.0) Build No 10.00154 on baseline-subtracted IR stretches using a custom two Gaussian function procedure:

$$GFP = y_0 + \frac{A_1}{w_1 * \sqrt{\pi/2}} * e^{\frac{(-2*(x-xc_1))^2}{w_1^2}} + \frac{A_2}{w_2 * \sqrt{\pi/2}} * e^{\frac{(-2*(x-xc_2))^2}{w_2^2}}$$

Where  $y_0$  indicates offset from baseline,  $A_x$  is peak area,  $w_x$  is peak width, and  $xc_x$  is peak center. In fitting,  $y_0$  and  $xc_x$  are shared from temperature to temperature, whereas  $A_x$  and  $w_x$  are allowed to relax to best fit the carboxylate stretch.

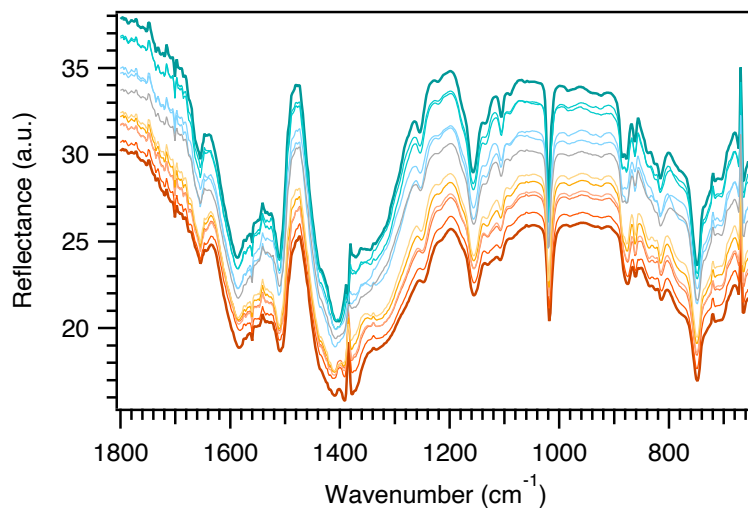


**Figure S2:** Variable-temperature diffuse reflectance infrared Fourier transform spectra (VT-DRIFTS) of UiO-66 under vacuum between 300 °C (red) and -100 °C (turquoise).

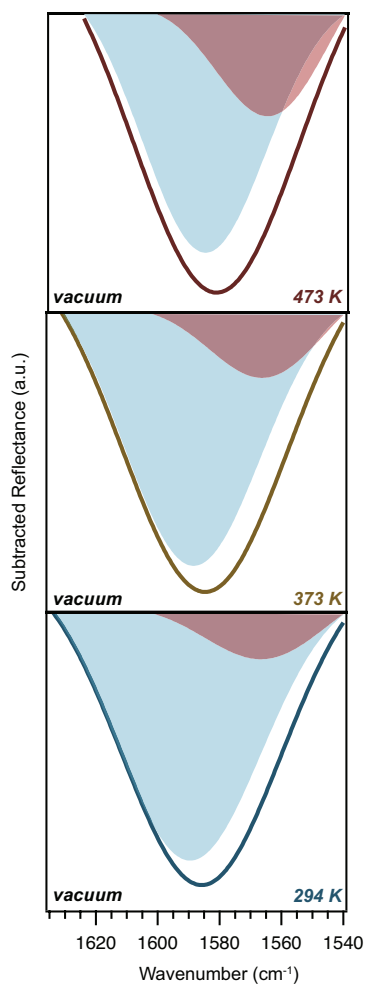


**Figure S3:** Global fitting analysis of the asymmetric stretch of UiO-66 under vacuum at three temperatures.

**Table S1:** Global fitting results for UiO-66 VT-DRIFTS under vacuum at three temperatures.

Plot	294 K	373 K	473 K
y0	$0.86 \pm 0.005$	$0.86 \pm 0.005$	$0.86 \pm 0.005$
xc1	$1590.57 \pm 5.21$	$1590.57 \pm 5.21$	$1590.57 \pm 5.21$
w1	$46.99 \pm 0.052$	$45.88 \pm 0.056$	$45.13 \pm 0.078$
A1	$-292.80 \pm 0.51$	$-256.18 \pm 0.49$	$-160.15 \pm 0.43$
xc2	$1565.83 \pm 5.84$	$1565.83 \pm 5.84$	$1565.83 \pm 5.84$
w2	$39.52 \pm 0.12$	$38.66 \pm 0.10$	$41.50 \pm 0.11$
A2	$-46.51 \pm 0.21$	$-67.44 \pm 0.21$	$-81.46 \pm 0.27$
R <sup>2</sup>	0.99990	0.99996	0.99999

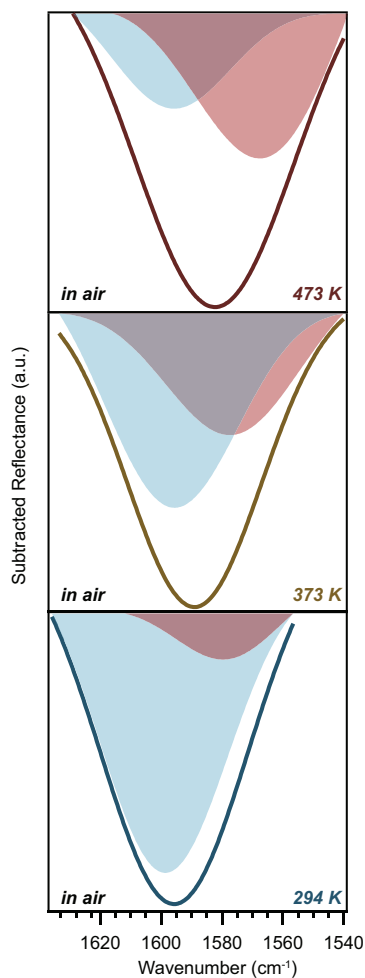


**Figure S4:** Global fitting analysis of the asymmetric stretch of UiO-66 in air at three temperatures.

**Table S2:** Global fitting results for UiO-66 VT-DRIFTS in air at three temperatures.

Plot	294 K	373 K	473 K
y0	2.12 ± 0.18	2.12 ± 0.18	2.12 ± 0.18
xc1	1599.11 ± 6.76	1599.11 ± 6.76	1599.11 ± 6.76
w1	42.20 ± 7.35	45.31 ± 6.46	40.65 ± 7.36
A1	-589.11 ± 233.03	-534.17 ± 287.59	-298.64 ± 357.14
xc2	1578.33 ± 6.84	1578.33 ± 6.84	1578.33 ± 6.84
w2	34.30 ± 4.11	45.78 ± 2.49	45.69 ± 1.11
A2	-104.33 ± 218.74	-343.76 ± 272.02	-799.72 ± 345.19
R <sup>2</sup>	0.9997	0.9977	0.9990

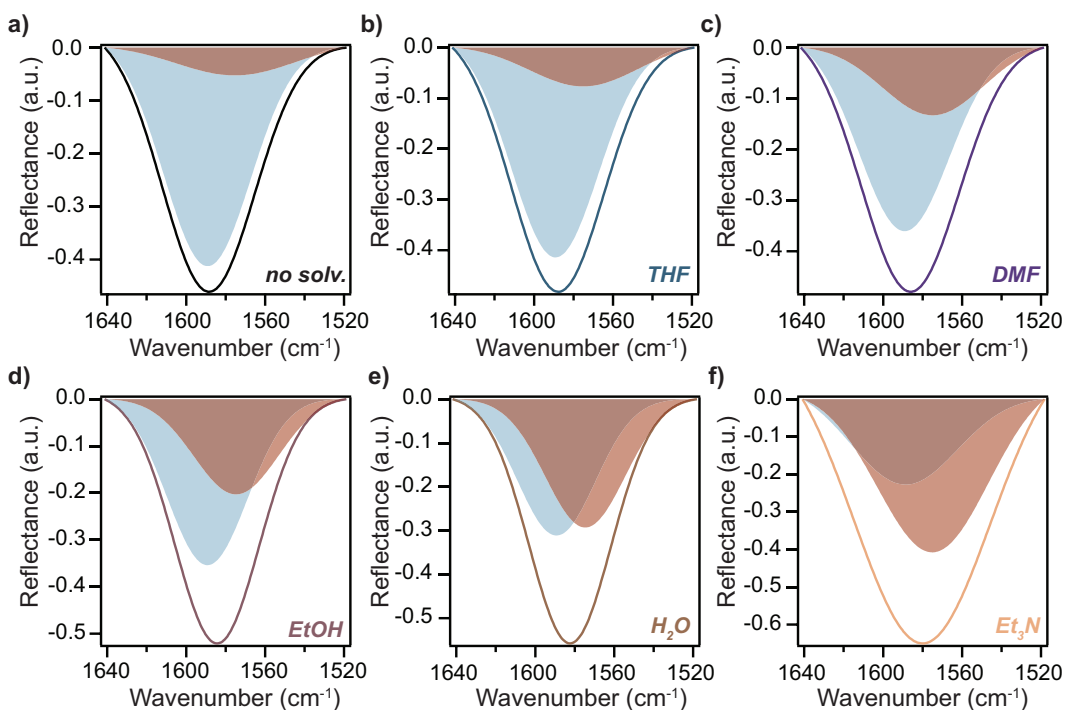


**Figure S5:** Asymmetric stretch of UiO-66 globally fit to “tight” (blue) and “loose” (red) states under exposure to various solvents.

**Table S3:** Global fitting results for UiO-66 VT-DRIFTS under exposure to vacuum, THF, DMF, EtOH, H<sub>2</sub>O, and Et<sub>3</sub>N.

Plot	no solv.	THF	DMF	EtOH	H <sub>2</sub> O	Et <sub>3</sub> N
y0	0.021 ± 1.59e-3	0.021 ± 1.59e-3				
xc1	1589.33 ± 0.48	1589.33 ± 0.48	1589.33 ± 0.48	1589.33 ± 0.48	1589.33 ± 0.48	1589.33 ± 0.48
w1	44.11 ± 0.95	43.94 ± 0.94	45.60 ± 0.84	40.69 ± 0.56	39.58 ± 1.10	54.00 ± 0.71
A1	-23.71 ± 2.29	-23.69 ± 2.98	-21.55 ± 4.69	-18.47 ± 5.70	-15.72 ± 7.65	-17.23 ± 16.15
xc2	1574.63 ± 7.41	1574.63 ± 7.41	1574.63 ± 7.41	1574.63 ± 7.41	1574.63 ± 7.41	1574.63 ± 7.41
w2	60.87 ± 5.78	55.08 ± 3.21	51.30 ± 1.76	42.86 ± 1.67	40.57 ± 1.63	56.20 ± 1.14
A2	-4.67 ± 2.43	-5.85 ± 3.13	-9.14 ± 4.84	-11.15 ± 5.84	-15.10 ± 7.81	-31.95 ± 16.33
R <sup>2</sup>	0.9996	0.9997	0.9997	0.9994	0.9992	0.9937

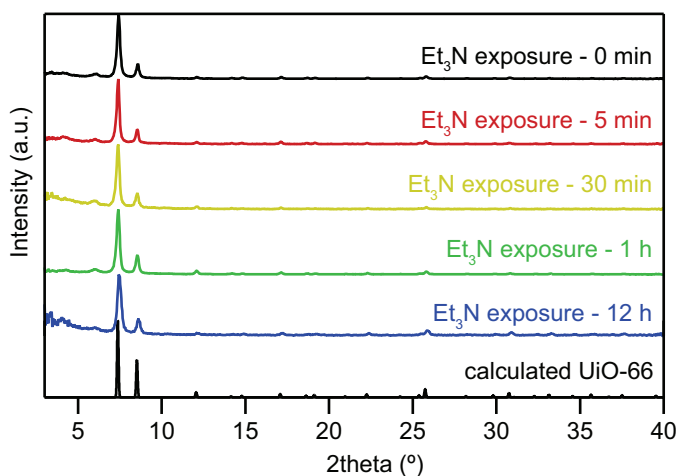


**Figure S6:** Experimental and simulated powder X-ray diffraction patterns for UiO-66 after being soaked in neat Et<sub>3</sub>N for periods of time.

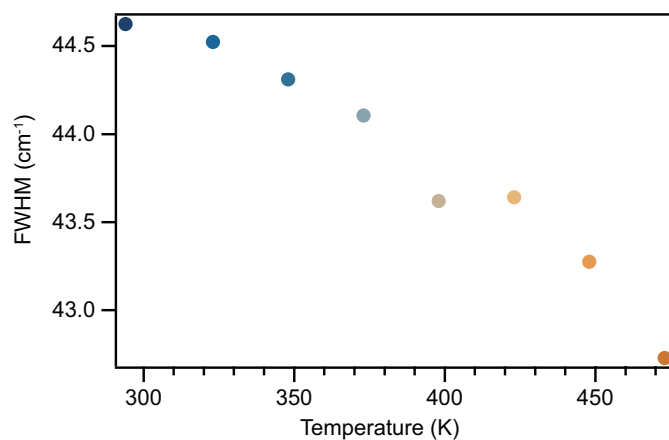


**Figure S7:** Comparison of FWHM values of baseline-subtracted DRIFTS data across examined temperature range and under vacuum.

**Table S4:** Stability constants for some metal-carbene and metal-pyridyl complexes, adapted from Ref. 4.

Material	$\ln K$
Pyridine/ZnTPP1(5,10,15,20-tetraphenylporphyrin)	9.9-8.1
bpy/Zn <sup>2+</sup>	12.4-12.2
phen/Zn <sup>2+</sup>	15.1-14.8
tpy/Zn <sup>2+</sup>	19.3-11.5
tpy/Fe <sup>2+</sup>	16.4
tpy/Co <sup>2+</sup>	19.3
tpy/Ni <sup>2+</sup>	24.6

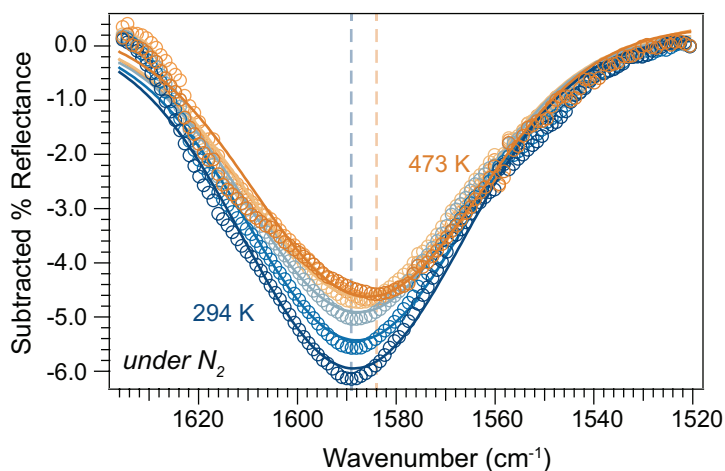


**Figure S8:** VT-DRIFTS data of UiO-66 under exposure to nitrogen. Dashed lines indicate peak minima at low and high temperatures.

**Table S5:** Global fitting results for UiO-66 VT-DRIFTS under exposure to dinitrogen.

Plot	294 K	323 K	373 K	423 K	473 K
y0	$6.17\text{E-}3 \pm 3.36\text{E-}6$				
xc1	$1591.78 \pm 7.76\text{E-}3$				
w1	$42.85792 \pm 7.58\text{E-}3$	$42.77811 \pm 1.02\text{E-}2$	$42.21008 \pm 1.54\text{E-}2$	$41.69048 \pm 0.119$	$44.42576 \pm 3.56\text{E-}2$
A1	$-162.81 \pm 1.35$	$-117.19 \pm 1.43$	$-73.98 \pm 1.38$	$-13.82 \pm 1.76$	$-39.00 \pm 1.70$
xc2	$1585.61 \pm 4.62\text{E-}2$				
w2	$42.86 \pm 7.29\text{E-}4$	$42.90 \pm 8.23\text{E-}4$	$42.46 \pm 9.16\text{E-}4$	$42.23 \pm 1.02\text{E-}3$	$44.83 \pm 9.31\text{E-}4$
A2	$-162.25 \pm 1.35$	$-179.34 \pm 1.43$	$-176.72 \pm 1.38$	$-235.33 \pm 1.76$	$-223.34 \pm 1.69$
R2	1.0000	1.0000	1.0000	1.0000	1.0000

**Table S6:** Environment-dependent flexibility constants at room temperature ( $\ln X$  when  $X = [\text{tight}]/[\text{loose}]$ ) of the asymmetric carboxylate stretch in UiO-66.

Solvent	Asymmetric peak ( $\text{cm}^{-1}$ )	$\ln X$ [asymmetric]
Vacuum	1589	1.8(4)
Air	1589	1.7(3)
N <sub>2</sub>	1589	1.6(6)
THF	1587	1.3(9)
DMF	1585	0.85(8)
EtOH	1581	0.50(5)
H <sub>2</sub> O	1579	0.04(0)
Et <sub>3</sub> N	1577	-0.61(7)

## References

- (1) Katz, M. J.; Brown, Z. J.; Colón, Y. J.; Siu, P. W.; Scheidt, K. A.; Snurr, R. Q.; Hupp, J. T.; Farha, O. K. A Facile Synthesis of UiO-66, UiO-67 and Their Derivatives. *Chem. Commun.* **2013**, *49* (82), 9449–9451. <https://doi.org/10.1039/C3CC46105J>.
- (2) Andreeva, A. B.; Le, K. N.; Chen, L.; Kellman, M. E.; Hendon, C. H.; Brozek, C. K. Soft Mode Metal-Linker Dynamics in Carboxylate MOFs Evidenced by Variable-Temperature Infrared Spectroscopy. *J. Am. Chem. Soc.* **2020**, *142* (45), 19291–19299. <https://doi.org/10.1021/jacs.0c09499>.
- (3) Andreeva, A. B.; Le, K. N.; Kadota, K.; Horike, S.; Hendon, C. H.; Brozek, C. K. Cooperativity and Metal–Linker Dynamics in Spin Crossover Framework Fe(1,2,3-Triazolate)<sub>2</sub>. *Chem. Mater.* **2021**, *33* (21), 8534–8545. <https://doi.org/10.1021/acs.chemmater.1c03143>.